3

Propyne on the (111) surfaces of Cu, Pt, Pd and Rh: adsorption sites, bonding mechanism and vibrational spectra

We have studied the adsorption of propyne on the (111) surfaces of Cu, Pt, Pd and Rh. On Cu (111), we have found that propyne adsorbs with its molecular plane perpendicular to the surface and bisecting a Cu-Cu bond. On Pt(111), Pd(111) and Rh(111), propyne prefers to sit on a 3-fold hollow site, with the C≡C axis parallel to a metal-metal bond and the molecular plane tilted away from the surface normal. The analysis of the DOS has allowed us to explain the apparently anomalous adsorption behaviour of propyne on the Cu surface. The simulation of the vibrational spectra has permitted us to corroborate and complete the experimental band assignment and confirm the adsorption site preference for propyne on Cu and Rh. Our calculations have also given a possible explanation for the presence of the MSSR-inactive C≡C stretch on Cu. For propyne on Pt and Pd,we have predicted the vibrational bands that will appear in the spectrum.

This chapter is organised as follows: section 3.1 is a literature review of the experimental and theoretical data available for propyne adsorbed on Cu(111), Pt(111), Pd(111) and Rh(111); section 3.2 discusses the geometry and vibrational spectrum of gas-phase propyne; section 3.3 presents the results for the adsorption of propyne on the (111) surfaces of Cu, Pt, Pd and Rh and discusses these results in terms of electronic and vibrational properties, through the analysis of the DOS and the simulated vibrational spectra; section 3.4 summarises the conclusions of this work.

3.1 Introduction

The chemistry of alkynes on metal surfaces exhibits a remarkable complexity that cannot be anticipated from the molecular structure and reactivity of the corresponding gas-phase molecules. The establishment and understanding of the microscopic mechanisms of these surface reactions requires the determination of the structure of the adsorbed molecules. Among the large number of surface analytical methods, vibrational spectroscopies (RAIRS and HREELS) are widely used in heterogeneous catalysis research [1-3]. The analysis of vibrational spectra, in particular, the assignment of the adsorbate vibrational modes, provides valuable information regarding the adsorbate structure, bonding modes and adsorption sites [4]. This information largely contributes to establish a first step towards the understanding of the elementary reaction steps occurring at the surface. The assignment of vibrational frequencies in terms of group functional frequencies is claimed to be very useful [6] although one must realize that this kind of analysis is based on rather classical arguments [7]. For adsorbates that retain most of their gas phase geometric and electronic structure, the assignment of vibrational frequencies is straightforward; it just requires direct comparison with available data for the gas phase molecule. However, when the interaction between the adsorbate and the surface implies a largely distorted structure for the adsorbate, the assignment becomes much more difficult. In some cases, it is possible to extract information from the IR spectra of the corresponding molecule obtained in different, but related, chemical environments such as inorganic complexes [8]. Nevertheless, this may lead to serious errors because the surface may strongly influence some particular normal modes [9]. Once vibrational bands are assigned, several hypotheses about the adsorption geometry are formed usually applying symmetry constrains and the *metal surface selection rule* (MSSR) [10,11]. Assuming the validity of this rule, it is usual to predict whether a given bond is parallel or not to the surface, on the basis of the presence or absence of the corresponding stretching band on the spectrum. Unfortunately, a lack of appreciation of the extent to which normal modes are composed of two or more coordinates produces errors in the assignation. Often, arguments based on Fermi resonances are to be invoked when a given band cannot be directly assigned.

Propyne ($CH_3C{\equiv}CH$) is one of the simplest hydrocarbons with more than two carbon atoms and an ideal candidate to study the structure and bonding modes of alkynes. In

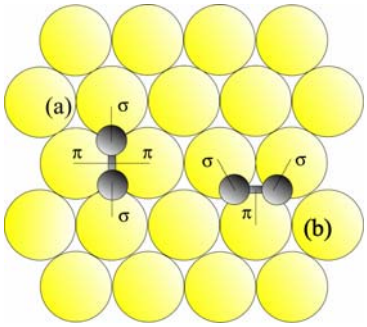

Scheme 3.1. Schematic diagram of the adsorption site of propyne on a (111) surface. Species (a) di-σ/di-π bonded and species (b) di-σ/π bonded.

principle, it is reasonable to expect propyne surface chemistry on metal surfaces to be similar to that of acetylene, as both molecules possess the same triple bond functionality. Besides, similarly to acetylene, propyne trimerises to form trimethylbenzene on the Pd(111) surface [12] and mainly undergoes dehydrogenation and further decomposition to surface carbon on both Pt(111) and Rh(111) surfaces [13,14]. However, it has been reported that the coupling reactions of propyne on Cu(111) are very different from those exhibited by acetylene. Actually, acetylene trimerises over Cu(111) even at low temperature while propyne mostly desorbs and undergoes dimerisation to benzene in a small fraction [15]. Structural studies have ascribed the low reactivity of propyne to steric repulsion between the methyl groups [16,17]. Elucidating the nature of the propyne-surface interaction, adsorption site, adsorption modes, packing arrangement and adsorption energies for these metals may also shed light on the causes of the different reactivity.

The carbon skeleton of propyne adsorbed on Cu(111) has been established by means of quantitative surface structure analysis based on the C(1s) Photoelectron Diffraction, PhD, technique. Likewise, LEED studies have also unambiguously established the long-range periodicity of propyne adsorbed on Cu(111) [16]. The propyne molecule binds to the copper surface in a di-σ/di-π adsorption mode (see **Scheme 3.1**) with its triple bond parallel to the surface in a cross-bridge position. A very important conclusion of this experimental study is that propyne arranges in a 4x√3 fashion. In a later study [18], McCash and co-workers have proposed a similar long-range periodicity for acetylene on Cu(111). Unfortunately, available structural information on the adsorption of propyne on Pt(111), Rh(111) and Pd(111) surfaces is relatively scarce. Comparison to acetylene adsorption mode suggests that propyne is also di-σ/π-bonded (see **Scheme 3.1**) to the Pt(111) surface [19]. A later temperature programmed desorption (TPD) study estimated a binding energy of ~–160 kJmol^{-1} at 0.25 ML coverage [13]. For propyne on Rh(111), an exhaustive experimental study [14] has proposed that this molecule binds to the Rh surface with its unsaturated bond approximately parallel to the surface forming a 2x2 ordered pattern but no detailed information about the adsorption mode and adsorption site is available. To the best of our knowledge there is no structural information available for propyne on Pd(111).

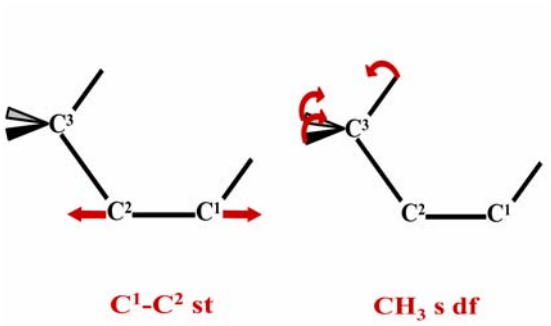

Scheme 3.2. Schematic representation of the C^1-C^2 stretch and the CH_3 symmetric deformation modes.

Experimental vibrational studies on Cu(111) [8] and Rh(111)[14] complete the structural information available. Despite the importance of these rigorous works, some bands have not been unambiguously assigned. In particular, the feature in the 1300–1400 cm^{-1} region has been attributed either to the $C^1{\equiv}C^2$ stretching ($C^1{\equiv}C^2$ st) or to the CH_3 symmetric deformation (CH_3 s st), see **Scheme 3.2**. On Cu(111), Chesters *et al.* assigned the band at 1361 cm^{-1} to the $C^1{\equiv}C^2$ stretch mode on the basis of a shift down to 1353 cm^{-1} upon deuteration of the 'acetylenic' hydrogen. Indeed, the EELS [20] and RAIR [8] spectra of acetylene on Cu(111) exhibits a strong peak at 1307 and 1294 cm^{-1} which has been also assigned to the $C^1{\equiv}C^2$ stretch. In these studies, the presence of the MSSR-inactive $C^1{\equiv}C^2$ stretch has been justified in terms of changes in dipole moment perpendicular to the surface arising from modification of the electron density near the $C^1{\equiv}C^2$ bond region produced by the vibrational mode parallel to the surface. McCash *et al*. [4] have suggested that this electron density change is enough to make this vibrational mode MSSR active and so intense. On the other hand, on Rh(111), Bent and co-workers [14] have assigned the 1370 cm^{-1} signal to the CH_3 symmetric deformation by comparison with the gas phase propyne spectrum. Later studies on Cu(110), Ni(111)[21], Pd(110)[22] have discussed the assignment of the bands in the 1300–1400 cm^{-1} region. On the Cu(110) and Ni(111) surfaces, Roberts *et al.*[21] have also assigned the 1354 and 1358 cm^{-1} features to the methyl symmetric deformation. They have based their assignment on the fact that methyl group deuteration produces a significant shift of these bands towards lower frequencies. In a similar way, Camplin *et al.* [22] have found that deuterium substitution on the acetylenic hydrogen does not affect the position of the 1343 cm^{-1} band on Pd(100) and thus they have assigned this peak to the methyl symmetric deformation although the same authors admit that the corresponding feature for propyne on Cu(111) may indeed correspond to the $C^1{\equiv}C^2$ stretching mode. They have proposed that in the last case the unit cell dimensions are such that the distance between two adjacent hollow sites matches that of the $C^1{\equiv}C^2$ bond of the chemisorbed propyne. This correspondence may allow the $C^1{\equiv}C^2$ stretch to become active at the expense of the methyl deformation.

Table 3.1. Calculated and experimental frequencies (in cm^{-1}) for the free propyne molecule

vibrational mode	calc. (ω_i)	exp. (ν_i)	$\Delta_{calc.-exp}$
CH st	3398	3334	64
CH_3 as st	3019	3008	–11
CH_3 s st	2976	2918[a]	58
$C^1{\equiv}C^2$ st	2172	2142	30
CH_3 as df	1424	1452	–28
CH_3 s df	1359	1382	–23
CH_3 ro + λ CCC b	1001	1053	–52
C^2-C^3 st	958	931	27
CH b	619	633	–14
CCC b	325	328	–3

Key: as, asymmetric; s, symmetric; st, stretching; df, deformation; ro, rocking; b, bending.
[a]Selected value. Fermi resonance with the CH_3 as df overtone. Experimental values at 2941 and 2882 cm^{-1}.

The need for a theoretical study is evidenced both by the lack of completeness of the available structural information and the existing disagreement in the literature regarding band assignment. Computational chemistry studies can be very useful in understanding the interaction of adsorbates with metal surfaces. The advantage of these studies is that they allow to obtain information that is difficult to measure experimentally such as adsorption energies for different structures or C−H distances. Moreover, the modern theoretical methods of electronic structure applied to surface science phenomena permit to obtain all the frequencies and, which is more important, they allow to get their relative intensities without further assumptions. Likewise, spectra for different isotopic substituted species —complicated and expensive to produce experimentally—can easily be obtained from theory with no significant additional cost.

For this chapter, we performed a series of self-consistent DFT calculations to asses the adsorption behaviour of propyne on four (111) metal surfaces: Cu, Pt, Pd and Rh. These surfaces were selected by the vast interest in catalysis of these four metals. The focus was on the adsorption site, electronic and vibrational properties, with a close comparison with the experimental results available. Our discussion is mainly focused on the comparison of the calculated vibrational spectra on the different metal surfaces.

3.2 Gas-phase propyne

First, for sake of comparison, the geometry of the gas phase molecules was optimised. We took a large box unit cell (15x15x15 $Å^3$) to avoid lateral interactions between periodic images. The results for the propyne molecule were close to the ones in previous experimental and theoretical studies [23]. The computed $C^1{\equiv}C^2$ and $C^2{-}C^3$ distances are

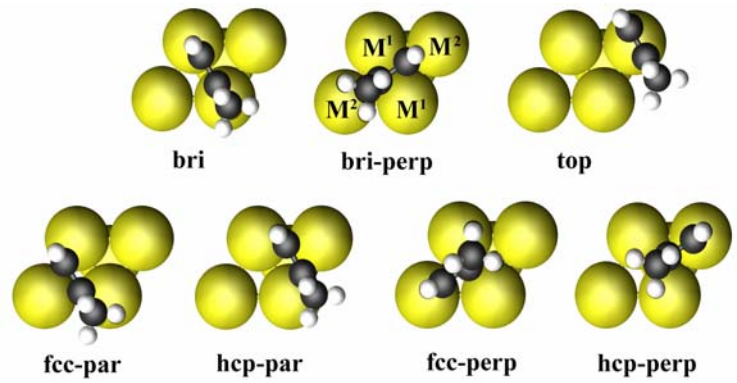

Figure 3.1. Scheme of adsorption structures for propyne on (111) metal surfaces.

1.21 Å, and 1.45 Å, respectively and the $C^1{\equiv}C^2{-}C^3$ angle is 180º as expected. The computed frequencies and assignments for gas phase propyne are displayed in **Table 3.1** where experimental results [24] have also been included for comparison. The agreement between experimental and calculated data is fairly good. Actually, the average deviation for the PW91 harmonic calculated vibrational frequencies (ω_i) with respect to the fundamental experimental values, ν_i, is of ~30 cm^{-1}.

The accurate assignment of the corresponding bands requires special care. In fact, upon deuteration couplings between group frequencies can appear, disappear or change their relative percentage. On deuteration of the 'acetylenic' hydrogen the CH st frequency shifts down and couples with the $C^1{\equiv}C^2$ st. McCash and co-workers [8] have also reported the existence of this coupling in the spectrum of physisorbed propyne on Cu(111). In this weak adsorption mode (physisorption) the molecule keeps its gas phase geometry and consequently its spectra can be compared to that of free propyne.

3.3 Adsorbed propyne

We identified at least seven different adsorption modes as possible starting points for geometry optimisations. The ball-and-stick representations are shown in **Figure 3.1**. The structures can be grossly classified as bridge (bri) when the C≡C is directly above a $M^1{-}M^1$ bond, hollow (fcc or hcp) when the molecule sits in a three-fold hollow site and top when the C≡C bond is directly above one metal atom. Depending on the angle formed by the C≡C axis and the $M^1{-}M^1$, we can distinguish two orientations namely parallel (par) and perpendicular (perp). Clotet and Pacchioni [25] have identified analogous structures for acetylene on Cu(111) and Pd(111). However, the lower symmetry of the propyne molecule duplicates some surface structures. For bri-perp two alternative situations exist depending on the position of the 'acetylenic' unit (C^1–H). The 'acetylenic' unit can sit on the fcc hollow site (see **Figure 3.1**) or on the hcp one. For sake of simplicity, we named them bri-

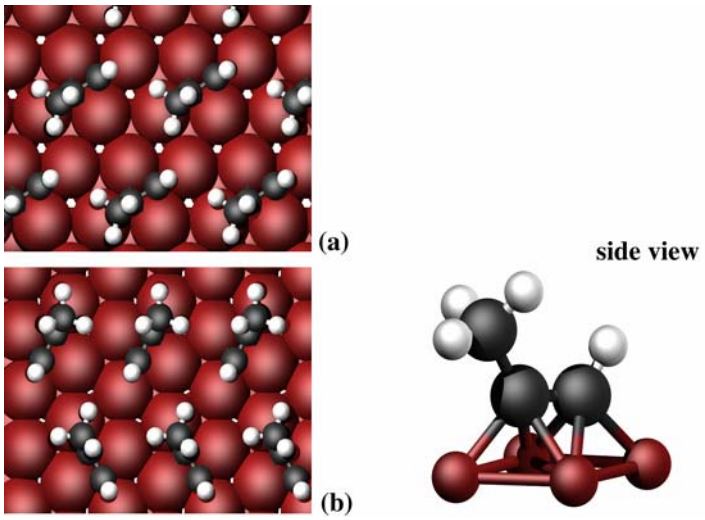

Figure 3.2. Bridge perpendicular (bri-perp) of propyne on Cu(111): 2x2 unit cell (a) and 4x√3-rect unit cell (b).

perp (C^1–H on fcc) and bri-perp' (C^1–H on hcp). Similarly, for fcc-perp and hcp-perp structures the C^1–H unit can be placed above the M^2 atom (**Figure 3.1**) or above the M^1–M^1 bond (not shown in the figure).

We performed the geometry optimisations using a 2x2 unit cell (associated with a molecular coverage of 0.25 ML). For propyne on Cu(111) a 4x√3 unit cell was also used to reproduce the LEED pattern observed experimentally [16]. We computed the adsorption energies with **equation 2.41** (**section 2.10**, **Chapter 2**). We also carried out frequency calculations with a 2x2 unit cell except for Cu, for which we used the experimental supercell [26]. Moreover, for the Rh surface, we also performed some calculations with a bigger supercell (two propyne molecules in a 2x4 unit cell).

3.3.1 Geometry, adsorption site preference and adsorption energy

Propyne on Cu(111). We consider first the case of propyne adsorbed on Cu(111). We found that only bri-perp structures are stable. These adsorption sites are fully compatible with the di-σ/di-π adsorption mode predicted by experiments. The adsorption energy is –73 kJmol^{-1} on the 2x2 unit cell (**Figure 3.2a**). The two possible orientations are strictly equivalent i.e. there is no difference in adsorption energy (nor in adsorption geometry, see below). The slab model permitted us to reproduce the long-range order proposed from LEED experiments (4x√3 unit cell, see **Figure 3.2b**) [16]. The adsorption energy is slightly larger on the 4x√3 unit cell (–98 kJmol^{-1}) than on the 2x2 one. The 4x√3 unit cell is the most stable adsorbed overlayer, as predicted from experiments.

We found no difference in the geometry of the two possible bri-perp structures (bond distances are equal up to the second decimal number). Moreover, both the 2x2 and the 4x√3 unit cell predicted identical adsorption geometry. This is a highly distorted propyne with the methyl group tilted away from the surface. The molecular C^1–C^2–C^3 plane is perpendicular to the surface (see **Figure 3.2** side view). The computed C^1–C^2 distance is 1.38 Å. Notice that the calculated value is well within the error bars of the experimental value which is 1.47 ± 0.16 Å. Similarly, the calculated C^2–C^3 distance is 1.51 Å to be compared with an experimental value of 1.57 ± 0.14Å and the C^1–C^2–C^3 bond angle is of 122º to be compared with a PhD value of 123 ± 7º (experimental values from ref. 16). There are several internal parameters that cannot be predicted by the diffraction experiments. Those are the bond distances and bond angles concerning the propyne hydrogen atoms. Not surprisingly, the C-H distances are all within 1.100±0.005Å where the error bars cannot be taken strictly as errors but as a measure of the dispersion of obtained results. The hydrogen methyl atoms are in a *cis* orientation, with one of the H atoms in C_3 almost in front of that in C_1 (**Figure 3.2**). Nevertheless, the rotation of the methyl group along the C^2–C^3 axis is almost free (less than 4 kJmol^{-1}). More important is the H– C^1–C^2 angle because it provides a measure of the C^1 hybridization. The calculated value is 120º and adds further support to a di-σ/di-π adsorption mode with C^1 and C^2 both on a sp^2-sp^3 like hybridisation. Here, it is important to point out that due to the lack of accuracy on PhD prediction of the bond distances that are nearly parallel to the surface. Toomes *et al.* [16] have not been able to distinguish between sp^2 and sp^3 hybridisation on C^1 and C^2. Chesters and McCash raised similar claims from the vibrational analysis [8]. The present values for the C^1–C^2 bond distance and H–C^1–C^2 and C^1–C^2–C^3bond angle strongly suggest an sp^2-sp^3 hybridisation. Indeed, this hybridisation is consistent with the di-σ/di-π coordination mode whereas it is difficult to understand the bonding of propyne to the surface with tetrahedral C^1 and C^2 atoms.

Finally, we discuss the vertical distances from the propyne carbon atoms to the surface plane and the surface relaxation. Experimentally it appears that both bri-perp and bri-perp' possibilities have the same probability and no structural differences are found. Hence, any deviation on the calculated geometry (or adsorption energy) of the two orientations could be taken as a measure of the model limitations. The vertical distances of C atoms to the surface in both the bri-perp and bri-perp' orientations are 1.39 (C^1) and 1.47 (C^2) to be compared with the experimental values, 1.44 ± 0.04 Å and 1.45 ± 0.04 Å, respectively. The vertical distances commented above are not changed when the two orientations within the 4x√3-rect unit cell were considered. Minor changes are observed on the Cu(111) surface upon adsorption of the propyne molecule. The three Cu atoms surrounding the C_2 move upward while the one directly under the 'acetylenic' unit moves inward, causing a slight corrugation of the metallic surface (< 3%). The changes on the second metal layer are even smaller. Only the hcp Cu atoms in the adsorption site move down, away from the carbon atom directly above.

Propyne on Pt(111). Among all the structures described above there are only two, fcc-par and hcp-par, which correspond to stable stationary points with minimum energy. The calculated adsorption energies for a coverage of 0.25 ML are –197 kJ mol^{-1} for the fcc-par

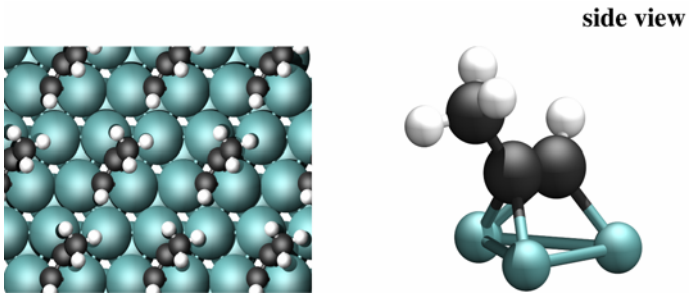

Figure 3.3. Hollow parallel (fcc-par) adsorption of propyne on Pt(111): 2x2 unit cell.

site and –193 kJ mol^{-1} for the hcp-par one. We can consider these surface structures equivalent as the energy difference between the fcc and hcp sites is only of 4 kJ mol^{-1}. On the other hand, this result is nicely compared with the TPD suggested value of ~–160 kJ mol^{-1} at 0.25 ML coverage [13]. Moreover, the energy barrier to diffusion perpendicular to the bridge is expected to be small based on the small energy gradients across the bridge computed during the geometry optimisation. It is worth to point out that the adsorption energy of propyne is smaller than the –218 kJ mol^{-1} [29] or –229 kJmol^{-1} [27] reported for the adsorption energy of the acetylene molecule also on Pt(111) using similar methods and models. The difference can be attributed to the presence of the extra methyl group, as in the case of adsorbed propylene compared to ethylene on Pt(111) [28] (see also **Chapter 4**).

On the Pt(111) surface, the molecule binds to two Pt atoms (di-σ bond) and forms an additional π bond with a third Pt (see **Figure 3.3**). The resulting structure is in a good agreement with the di-σ/π one suggested by early experimental studies [19]. Due to the extra π-bond, the molecular C^1–C^2–C^3 plane is tilted away from the surface normal of ~ 15º (side view, **Figure 3.3**). Both minimum energy structures have similar adsorption energies and rather similar geometries indicating that the bonding is dominated by the three surface atoms defining a hollow site with little influence of the atoms in the second and third layers. Propyne adsorbs on Pt(111) with the C^1–C^2 bond almost parallel to the surface and the methyl group pointing outwards the metal surface with a C^1–C^2–C^3 angle of 125º (124º) for the fcc-par (hcp-par) structure. The C^2–C^3 is 1.50 Å for both surface minima and we did not find significant differences in the C–H bond distances (~1.10 Å). The C^1–C^2 distances are 1.39 Å and 1.40 Å for the fcc and hcp modes, respectively. This value can be used as a measure of the activation of the C^1–C^2 bond. Evidently, the C^1–C^2 distance is rather elongated from the calculated value for the gas-phase propyne (1.21 Å) and lies between the usual distances for a double (1.34 Å, gas-phase propylene) and a single bond (1.54 Å, gas-phase propane). The significant elongation of the C^1–C^2 distance indicates a considerable loss of triple-bond character upon adsorption. Similar elongation of the triple bond (1.40 Å) has been recently reported for acetylene on the Pt(111) surface [29]. The 123º value for the H–C^1–C^2 angle adds further support to a di-σ/π adsorption mode with C^1 and C^2 both in a sp^2–sp^3 like hybridisation.

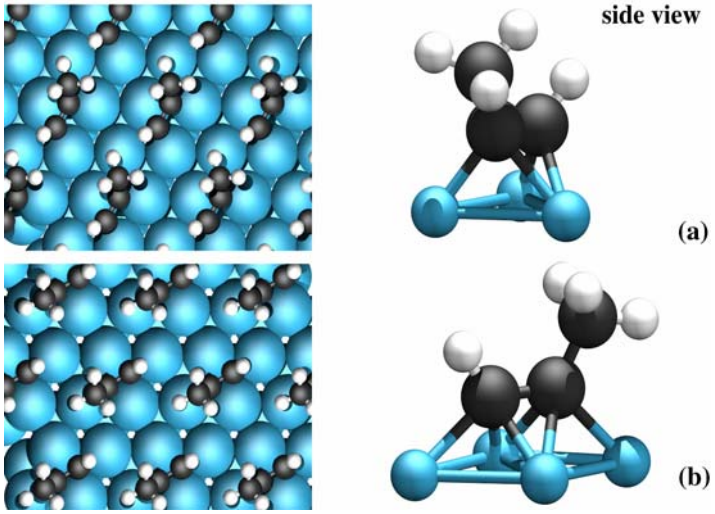

Figure 3.4. Adsorption of propyne on Rh(111): 2x2 unit cell; hcp-par (a) and bri-perp' (b).

The vertical distances of C^1 and C^2 atoms to the metal surface are 1.44 Å and 1.52 Å respectively for the fcc-par and 1.45 Å (C^1) and 1.53 Å (C^2) for the hcp-par mode. As for the Cu(111) surface, minor changes are observed on the Pt(111) one upon adsorption of propyne. The surface metal atoms in the adsorption site move slightly upward (~0.12 - 0.24 Å) to the adsorbed molecule whereas the fourth atom in the unit cell moves inward (~0.1 Å). This produces a small surface corrugation. The relaxation of atoms in the second metal layer is even smaller. Therefore, the space between to consecutive metal layers increases in ~4%.

Propyne on Pd(111). When adsorption takes place on the Pd(111) surface, we obtained the same geometrical trends we found for the adsorption on the Pt(111) surface. Among all the initial structures tested, only the fcc-par and the hcp-par adsorption modes led to stable structures. Similarly to Pt, we can consider the two minima *quasi*-degenerate as the adsorption energies are –160 and –161 kJ mol^{-1} for the fcc and hcp adsorption modes, respectively. There appears to be no difference between binding at fcc *versus* hcp sites; that is, the presence or absence of the second layer Pd atom, below the hollow site does not affect the adsorption. In this case, the adsorption energy is also smaller than the computed one for acetylene on Pd (-196 kJ mol^{-1}) [29].

Both minima also have quite close geometries. The molecule binds to the metal surface in a di-σ/π fashion with the molecular plane slightly tilted from the surface normal (~13º). The C^1–C^2 distance is 1.36 Å for the fcc-par and 1.37 Å for the hcp-par adsorption mode. DFT periodic calculations carried out by Mittendorfer and co-workers [29] predict the same C^1–C^2 distance for the acetylene molecule adsorbed on Pd(111), which is indeed close to the experimental value of 1.34 Å [30]. The calculated H–C^1–C^2 and C^1–C^2–C^3angles are

Table 3.2. Computed propyne adsorption energies (in $kJmol^{-1}$) and geometries (distances in Å, angles in degrees) for the most stable structures on the (111) surface of Cu, Pt, Pd and Rh

	Cu	**Pt**	**Pd**	**Rh**	
Adsorption mode	bri-perp	fcc-par	fcc-par	hcp-par	bri-perp'
Adsorption energy	–98	–197	–161	–226	–209
C^1–C^2 distance	1.38	1.39	1.36	1.39	1.42
C^2–C^1–H angle	123	123	125	123	120
M^1–C^1 /C^2 distance	2.13 /2.13	2.01/2.02	2.00/2.03	2.04/2.01	2.11/2.20
M^2–C^1 /C^2 distance	2.04/2.06	2.20/2.25	2.19/2.22	2.20/2.16	2.19/2.18
Tilt[a]	0	16	14	15	0

[a]Angle of the molecular plane of propyne with respect to the surface normal.

125º and 127º for both surface minima. These values strongly suggest a sp^2 to sp^3 hybridisation consistent with the di-σ/π coordination mode.

For the fcc-par structure the height of C^1 and C^2 atoms above the metal surface is 1.45 Å and 1.55 Å, respectively. These distances are only 0.01 Å longer for the hcp-par structure. The Pd surface relaxation is ~3%.

Propyne on Rh(111). The computed adsorption behaviour of propyne on Rh(111) follow similar trends to the results for the other metals. We performed the calculations using a 2x2 unit cell. Indeed, Somorjai and co-workers [14] have suggested that this is the pattern propyne forms on the Rh surface. On this metal surface, four different adsorption modes correspond to minima: hollow-par (fcc and hcp) and the bri-perp structures (see **Figure 3.4**). The hollow-par adsorption sites are the most stable ones with adsorption energies of –226 $kJmol^{-1}$ and –216 $kJmol^{-1}$ for the hcp-par and fcc-par structures, respectively. Contrary to Pt and Pd, on the Rh surface the adsorption on the hcp hollow site is slightly favoured compared to the adsorption on the fcc. Previous theoretical studies have pointed out this site preference for molecules (such as acetylene or NO) and atoms (C, N) [27,31]. The bri-perp surface structures have somehow lower binding energies (–207 for bri-perp and –209 $kJmol^{-1}$ for bri-perp'). The energy difference between bri-perp adsorption mode and the hcp-par surface structure is smaller than 20 $kJmol^{-1}$. This difference is not big enough to be conclusive. In fact, a recent study for CO adsorption on Pt(111) has shown that GGA-DFT yields an error of 10–20 $kJmol^{-1}$ for the comparison of adsorption sites [32], predicting an erroneous binding site. Hence, the simulation of the vibrational spectrum may be of great importance to confirm the site preference obtained from total energy calculations (see **section 3.3.3**). Allendorf and co-workers [27] have obtained similar results for acetylene on Rh(111). Both hollow-par and bri-perp structures lie in a small range of energies and the most stable adsorption site is also the hcp-par (–258 $kJmol^{-1}$).

Although the adsorption energies are rather similar, the differences in geometry are not negligible. The molecular geometry is clearly less distorted on the hollow-par than on the bri-perp structures. In fact, the calculated C^1–C^2 distance is 1.39 Å and the H−C^1–C^2 and C^1–C^2–C^3 angles are 123º and 124º for both surface minima (hcp and fcc) to be compared with 1.42 Å, 125º and 127º obtained for the bridge perpendicular minima (bri-perp and bri-

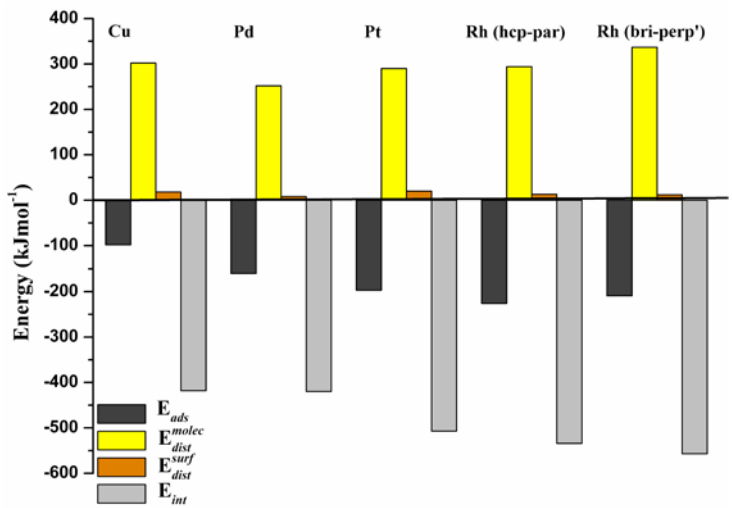

Figure 3.5. Decomposition of the adsorption energy for the most stable adsorption mode on the (111) surfaces of Cu, Pd, Pt, and Rh. Adsorption energy (dark grey), distortion energy of the molecule (yellow), distortion energy of the surface (orange) and interaction energy (light grey).

perp'). There are also rather important differences in the vertical distances. For the hollow-par structures the height of C^1 and C^2 atoms above the metal surface is 1.53 Å and 1.62 Å, respectively. However, these values are reduced to 1.40 Å (C^1) and 1.49 Å (C^2) for the bri-perp structures.

Similarly to the other metals studied, there are no significant changes in the geometry of the metal surface on adsorption. For all the minima, the surface relaxation is <4%. As expected, the changes in the Rh(111) surface are similar to those observed in Pt(111) and in Cu (111) for the hollow-par and for the bri-perp's structure, respectively.

Table 3.2 summarises the results described above. It provides a list of adsorption energies and geometric parameters for the most stable adsorption mode on each metal surface. For the Rh surface, we also included the bri-perp' surface structure. We can explain the variation of adsorption energies on Cu (–98 $kJmol^{-1}$), Pd (–161 $kJmol^{-1}$), Pt (–197 $kJmol^{-1}$) and Rh (–209 $kJmol^{-1}$ for the bri-perp' structure and –226 $kJmol^{-1}$ for the hcp-par adsorption mode) in terms of geometric distortions and electronic interactions. We can decompose the adsorption energy in three terms (**Figure 3.5**): the distortion energy of the surface, related to the distortion of the first metallic layers; the distortion energy of the molecule, i.e the energy necessary to distort the molecule from its gas phase geometry to the adsorption geometry; and the interaction energy between the distorted molecule and the distorted surface. The distortion energy of the surface is a minor contribution. In all the cases, this value is smaller than 20 $kJmol^{-1}$ in good agreement with the small changes observed on the metal surface on adsorption (see above). The distortion energy of propyne increases following: Pd (252 $kJmol^{-1}$) < Pt (290 $kJmol^{-1}$) ≈ Rh (294 $kJmol^{-1}$, hcp-par) ≈ Cu (302 $kJmol^{-1}$) < Rh (337 $kJmol^{-1}$, bri-perp'). These values reflect the increasing deformation

of the molecular geometry upon adsorption. The hollow-par adsorption structures of Pt and Rh have surprisingly close geometries. On the other hand, the geometry of the bri-perp's structure differs from those obtained for propyne adsorbed on Cu(111). Distinctly, the distortion of the molecular geometry is higher on Rh. In fact, we can consider the changes in C^1–C^2 bond length and the H–C^1–C^2 angle as an indicative of the 'activation' of the molecule. The more elongated is the C^1–C^2 distance and the smaller is the H–C^1–C^2 angle the higher is the activation. The interaction energy between the two distorted fragments increases from Cu (–418 $kJmol^{-1}$) ≈ Pd (–420 $kJmol^{-1}$) < Pt (–507 $kJmol^{-1}$) < Rh (hcp-par, –534 $kJmol^{-1}$) to Rh (bri-perp, –557 $kJmol^{-1}$). The interaction energy is clearly stronger on Rh and Pt than on Pd and Cu. The rather strong activation and the high interaction of propyne on Pt and Rh cause the adsorbed molecule to be susceptible of decomposition. Our calculations are in good agreement with the experimental results [13,14]. Unfortunately, our results do not give any indication as to why propyne trimerises on Pd and dimerises on Cu. Experimental [15] and theoretical [17] studies have proposed the key intermediates and the mechanism for propyne dimerisation on Cu. The study of the reaction intermediates and the possible reaction pathways on both metal surfaces is necessary to establish the causes of the differences observed.

3.3.2 Electronic analysis

In the foregoing section, we have discussed the relative stability and adsorption site preference on the Cu, Pt, Pd and Rh surfaces. The analysis of the projected density of states (PDOS) with the simple frontier orbital model [33] can help us to understand the bonding mechanism. **Figures 3.6** and **Figure 3.7** show the PDOS on the atomic orbital of C^1 and the surface metal atoms. For Cu, Pt, and Pd we only considered the most stable structures whereas for Rh both hcp-par and bri-perp adsorption modes are analysed. In hollow-par and bri-perp's adsorption modes the orbitals into play are mainly the p_x and p_z of the C atom (π system) and the d_{xz}, d_{yz} and d_z^2 metal orbitals (d-band). However, we also investigated the contribution of the sp-band to the propyne-surface interaction. For these metals, the sp-band doses not strongly contribute to the adsorbate-surface interaction except for Cu (see discussion below).

First of all, we discuss the isolated propyne molecule. In each graphic, window (1) presents the PDOS on the p_x and p_z orbitals of the C^1 atom of both the gas phase (dotted line) and the 'distorted' propyne (full line) —i.e the isolated molecule but in the adsorption geometry—. The highest occupied molecular orbitals (HOMO) and the lowest unoccupied molecular orbitals (LUMO) are doubly degenerate in the gas phase. On adsorption, the molecular distortion results in a symmetry lowering and in a marked reduction of the HOMO-LUMO (H–L) gap. It is well known that the energy difference between the HOMO and the LUMO is directly linked to the distortion of the molecule: the higher is the distortion the smaller is the H–L gap. **Figure 3.8** shows that there is a clear linear relationship between the H–L gap and the energy cost to distort the propyne molecule from its gas phase geometry to the adsoption geometry. Moreover, this distortion causes an increase of the mixing between p_x and p_z orbitals with C orbitals of 'pure' σ character. As a result of this mixing two peaks grow in the 4.5–7.5 eV range.

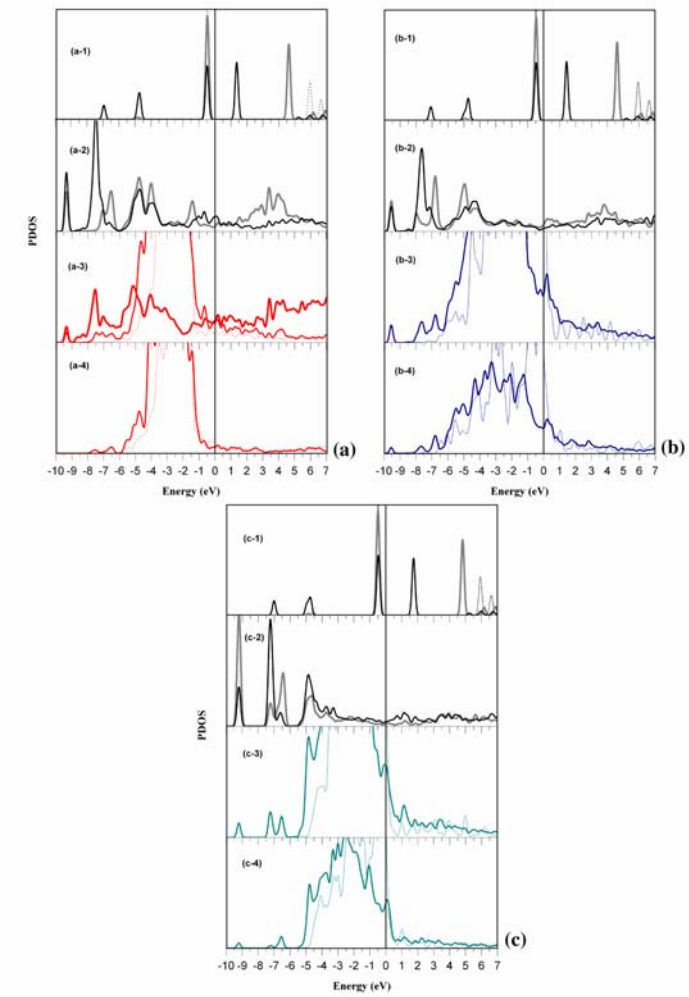

Figure 3.6. Density of states projected (PDOS) on the p_x (gray) and p_z (black) atomic orbitals of propyne and the d_{z^2} and $d_{xz}+d_{yz}$ of Cu(111) (a); Pt(111) (b) and Pd(111)(c). Window 1, propyne in the gas phase (dotted line) and isolated propyne distorted as in the surface structure (full line). Window 2 adsorbed propyne. Window 3, d_{z^2} of the clean (dotted line) and 'interacting' (full line) metal surface. For Cu, the sp-band is also depicted in window 3 (thick line). Window 4, $d_{xz}+d_{yz}$ of the bare surface (dotted line) and with adsorbed propyne (full line). Fermi level is taken as zero.

Due to the interaction with the metal surface, the adsorbate contributions are broadened and pushed to lower energies (see window (2)). The more 'dilute' the p_x and p_z contributions are, the stronger is the interaction with the metal surface. This is evident if we

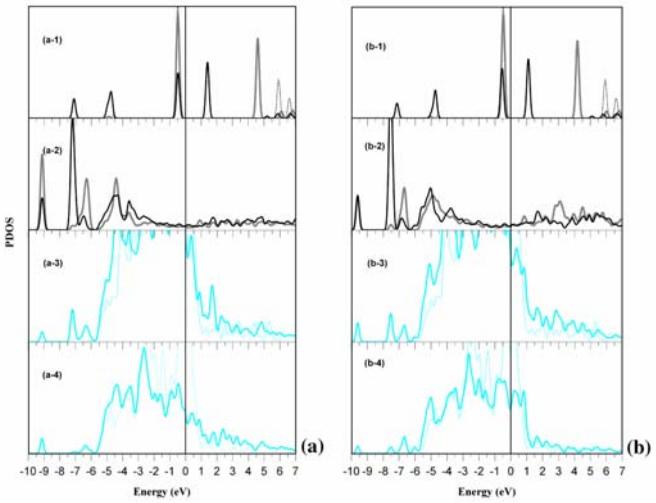

Figure 3.7. Density of states projected (PDOS) on the p_x (grey) and p_z (black) atomic orbitals of propyne and the d_{z^2} and $d_{xz}+d_{yz}$ of Rh(111): hcp-par (a) and bri-perp'(b). Window 1, propyne in the gas phase (dotted line) and isolated propyne distorted as in the surface structure (full line). Window 2 adsorbed propyne. Window 3, d_{z^2} of the clean (dotted line) and 'interacting' (full line) metal surface. Window 4, $d_{xz}+d_{yz}$ of the bare surface (dotted line) and with adsorbed propyne (full line). Fermi level is taken as zero.

compare, for example, the adsorption of propyne on Pt (interaction energy –507 $kJmol^{-1}$) and Pd (interaction energy –420 $kJmol^{-1}$), see **Figures 3.6b** and **c**. We can invoke similar arguments to compare the two stable adsorption structures on Rh (**Figures 3.7a-b**).

Windows (3) and (4) show the PDOS on the d_{xz} + d_{yz} and th d_z^2 orbitals for the clean (dotted line) and 'interacting' (full line) metal surface. For Cu (**Figure 3.6a**) we also included the sp-band. Notice that the Cu d-band remains rather narrow upon adsorption. Consequently, the interaction with the H–L contributions of propyne is less effective. On the other hand, there is a noticeable interaction of these orbitals with the sp-band. This interaction is evidenced by the matching energies between the sp contributions and p_x and p_z contributions. There is an important overlap of the s metal contributions and the π C–C antibonding orbitals, which strengthens the surface-adsorbate binding (peaks in the range 2–4.5 eV). These results are analogous to those of acetylene on the Cu(111) surface. Indeed, Clotet and Pacchioni [25] have proposed that the sp-band participates substantially in the acetylene binding to Cu.

For Pt, Pd and Rh, (**Figures 3.6b-c** and **Figure 3.7a-b**, respectively) the interaction takes place mainly with the d_{xz}, d_{yz} and d_z^2 bands. Upon adsorption, the d contributions just below the Fermi level (taken as zero energy) are rather reduced, while new contributions appear at low energies (below the d-band bottom) and above the Fermi level from the bonding and antibonding contributions with the p_x and p_z orbitals. The interaction primarily takes place with the HOMO of propyne. However, there is a non negligible contribution of

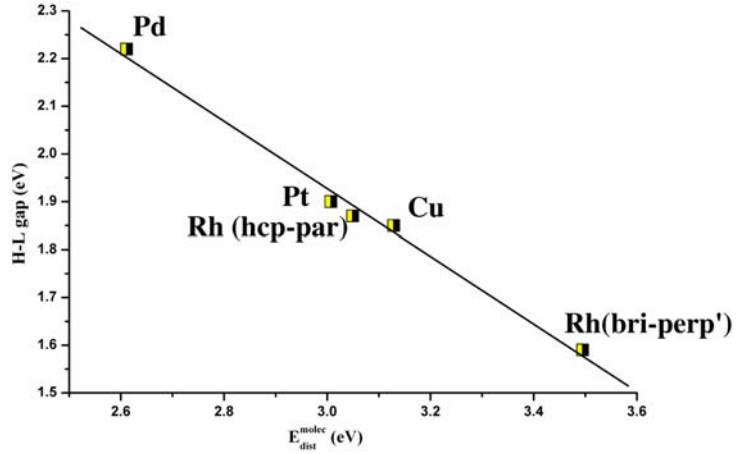

Figure 3.8. HOMO–LUMO gap *vs*. the distortion energy of the molecule. Energies in eV.

the propyne LUMO. The surface-metal interaction increases in the order Pd < Pt < Rh, well in line with the increase of the d-bandwidth. The greater expansion of the d orbitals favours the overlap of the metal and adsorbate states. The 4d orbitals of Pd are narrower than the 5d orbitals of Pt. Rh (a more electropositive metal) has higher d states and more diffuse orbitals. Moreover, the stronger distortion of the molecular geometry of adsorbed propyne (Rh > Pt > Pd) also favours the overlap between the adsorbate and the d metal band and propitiates the interaction.

The unique adsorption behaviour of propyne on Cu arises from the singular adsorbate-surface interaction.

3.3.3 Vibrational spectra

The system propyne/M(111) surface belongs to the C_1 symmetry (see **section 3.3.1**). Therefore, all the vibrational modes can be active. However, when the calculated frequencies are compared with the IR or HREELS spectra, the metal surface selection rule has to be taken into account [10,11]. Only modes that produce a significant change in the dipole moment perpendicular to the metal surface are active (for further details see **Chapter 2, section 2.6**)

Although the adsorbed system does not exhibit any particular symmetry, the propyne molecule has a local symmetry close to C_s. Actually, we can consider that the 'acetylenic' and the methyl hydrogens lie in the plane formed by the three C atoms because the deviation from this plane is always smaller than 5º. Thus, for sake of simplicity, we used the C_s local symmetry and the group frequencies displayed in **Figure 3.9** to assign the bands. Our goal is to 'translate' the computed normal modes into 'functional group' modes. Sometimes vibrational normal modes are the sum of two (even more) functional group modes. So, we will use a '+' sign to indicate that two (or more) functional groups couple

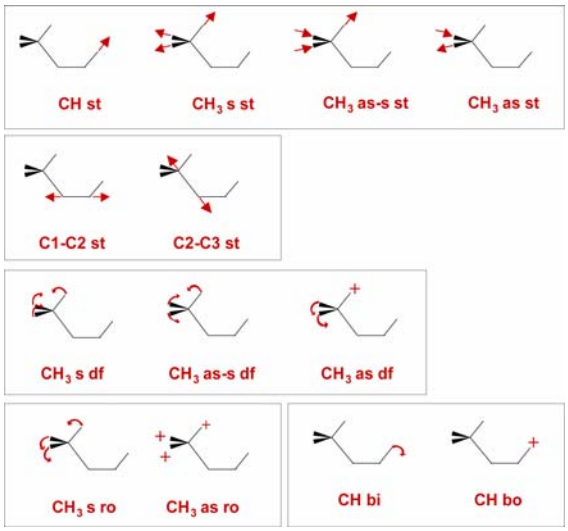

Figure 3.9. Notation used in the band assignation. Key: as, asymmetric; s, symmetric; st, stretching; bi, bending in-plane; bo, bending out-of-plane; ro, rocking; df, deformation. The as-s notation corresponds to nuclear displacements symmetric to molecular plane.

(or sum) in the sense displayed in **Figure 3.9** and a '–' sign when they couple in opposite sense (i.e. displacement vectors of each functional group move in opposite sense).

Propyne on Cu(111). The experimental RAIR spectrum of propyne on Cu(111) [8] has four bands in the CH stretching region (2923, 2883, 2855 and 2828 cm^{-1}) and a quite strong feature at 1361 cm^{-1}. Chesters and McCash [8] have assigned the band at 2923 cm^{-1} to the CH_3 as st, the one at 2883 cm^{-1} to the CH_3 s st, the feature at 2855 cm^{-1} to the 'acetylenic' hydrogen stretch (CH st), the peak at 2828 cm^{-1} to the CH_3 s st coupled with the overtone of the CH_3 s df (Fermi resonance) and the band at 1361 cm^{-1} to the C^1–C^2 st. Unfortunately, the resolution of this spectrum is rather low and the authors have only assigned the main bands with no attempt to resolve the numerous shoulders. To corroborate and complete the experimental assignment, we computed the vibrational frequencies of propyne on Cu(111) using two different models: a 2x√3 supercell (1 molecule per unit cell) and the 4x√3 supercell (experimental LEED pattern [16], 2 molecules per unit cell).

First, we computed the vibrational frequencies of the bri-perp and bri-perp' using the 2x√3 cell. **Table 3.3** shows these results. This model reproduces rather well the CH stretching region: CH_3 as st (3020/3024 cm^{-1}), CH_3 as-s st (3004/2997 cm^{-1}), CH st (2944/2944 cm^{-1}) and CH_3 s st (2923/2927 cm^{-1}). Here, the values in parenthesis correspond to the bri-perp and bri-perp' orientations, respectively. The anharmonic effects are obvious in the comparison between computed and experimental frequencies, with a discrepancy of the same range as in the gas phase propyne (see **section 3.2**). The model also reproduces rather well the band intensities in the 2900–3100 cm^{-1} region. The CH_3 s st is the most intense feature followed by the CH st and the CH_3 as-s st mode. The CH_3 as st has an

Table 3.3. Computed frequencies (in cm^{-1}) for propyne (CH_3CCH) on Cu(111)

vibrational mode	2x√3		4x√3	
	ω_i	I_i[a]	ω_i	I_i[a]
A (CH_3 as st)	3020	0.1	3018	0.2
B (CH_3 as st)	3024	0.1	3008	0.2
B (CH_3 as-s st)	2997	0.6	2992	1.7
A (CH_3 as-s st)	3004	0.7	2989	0.7
B (CH st)	2944	3.7	2935	6.5
A (CH st)	2944	3.5	2930	4.4
A (CH_3 s st) + (CH3 s st)	2923	18.0	2920	25.8
B (CH_3 s st) – (CH3 s st)	2927	14.2	2918	5.0
A (CH_3 as-s df)	1427	0.1	1477	0.2
B (CH_3 as-s df)	1430	0.1	1429	0.0
A (CH_3 as df)	1410	0.0	1422	0.1
B (CH_3 as df)	1413	0.1	1413	0.0
B (C^1–C^2 st – CH_3 s df) – A(C^1–C^2 st – CH_3 s df)	1356	2.4	1354	1.2
A (C^1–C^2 st – CH_3 s df)+ B(C^1–C^2 st – CH_3 s df)	1357	2.0	1350	5.9
B (CH_3 s df + C^1-C^2 st)	1327	0.4	1330	0.2
A (CH_3 s df + C^1-C^2 st)	1328	0.1	1325	0.9

Key: as, asymmetric; s, symmetric; st, stretching; df, deformation; ro, rocking; b, bending.
[a]IR intensities in $Kmmol^{-1}$. A and B account for the bri-perp and bri-perp'structures, respectively. In red, inter-molecular coupling.

intensity close to zero (see **Table 3.3**). The outstanding difference arises from the band order. In the experimental spectrum the CH_3 s st mode appears at higher frequency than the CH st mode whereas it appears at a lower frequency in the simulated spectrum. This order reversal may be ascribed to the presence of the CH_3 s df overtone in the experiment, which, obviously, is not explicitly included in the harmonic frequency calculations. However, our calculation have confirmed that propyne adsorbs on Cu(111) on two distinct adsorption sites. Thus, it may be interesting to study how the existence on the surface of molecules adsorbed on different orientations (bri-perp and bri-perp') influences the frequencies and intensities. The exhaustive study of Chesters and McCash [8] has neglected this effect because the experimental spectrum has been performed and assigned thirteen years before the LEED pattern has been resolved [16].

In the 1300–1500 cm^{-1} region, we assign the very weak feature at 1427/1430 cm^{-1} to the CH_3 as-s st. The peak at 1357/1356 cm^{-1} is the only band in this region with a significant intensity. The agreement with the experiment is excellent. Cherters and McCash [8] have assigned the feature at 1361 cm^{-1} to the C^1–C^2 st. However, we assign this feature to the CH_3 s df coupled to the C^1–C^2 st. mode. Interestingly enough, this coupling produces two bands with very different intensities. Actually, the negative coupling (1356/1357 cm^{-1}, C^1–C^2 st – CH_3 s st) is up to eighteen times more intense than the positive coupling (1327/1328 cm^{-1}, CH_3 s st + C^1–C^2 st). Here, positive and negative refers to notation in **Figure 3.9**.

It is not easy to discuss the change in frequency upon adsorption because it is not always possible to link the vibrational modes in the adsorbed molecule to those in the gas

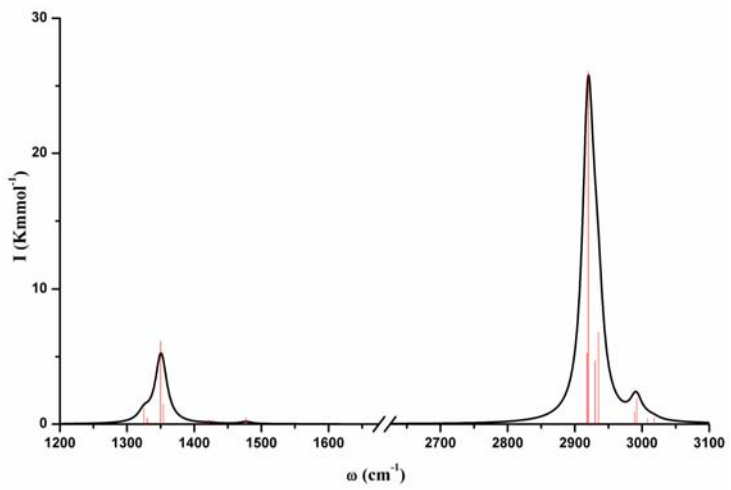

Figure 3.10. Simulated vibrational spectrum for propyne/Cu(111) for the 4x√3 unit cell. Obtained using Lorentzian functions, with a bandwidth of 20 cm^{-1} and a resolution of 0.5 cm^{-1}.

phase species. However, some general trends can be observed. On adsorption there are no significant changes in the methyl stretching and deformation frequencies well in line with the absence of geometric changes. On the other hand, the CH st and the C^1–C^2 st frequencies decrease drastically (~450 and ~800 cm^{-1}, respectively). We can consider these differences as a measure of the activation of the C≡C bond. Computed frequencies support the sp^2–sp^3 hybridisation inferred from structural data.

After the analysis of the local modes, we will discuss the results that we obtained with the 4x√3 model. **Figure 3.10** shows the simulated vibrational spectrum. In the forthcoming paragraphs, we will focus our attention in the analysis of the possible inter-molecular couplings and the isotopic effects. There are no important changes in both frequencies and intensities in the CH stretching region except for the CH_3 s st mode. The coupling between the CH_3 s st modes of the two molecules present in the unit cell produces two bands with a very different intensity (26/5, **Table 3.3**). The intense peak corresponds to the vibrational mode where all the methyl hydrogen atoms move in the same sense and the weak feature corresponds to the normal mode where the H atoms move in the opposite sense.

The two models predict the same band order in the 2900–3100 cm^{-1} region. Therefore, we can exclude that the coupling between functional group modes of molecules adsorbed in different adsorption sites causes the reverse order of the CH_3 s st and the CH st modes. Thus, we confirm the assignment of Chesters and McCash [8].

The results for the 1300–1500 cm^{-1} region are also well in line with those obtained with the 2x√3 unit cell. The peaks at 1350/1354 cm^{-1} and 1325/1330 cm^{-1} are also assigned to the negative and positive coupling between the CH_3 s df and the C^1C^2 st mode. However, there is a small shift (< 7 cm^{-1}) of these bands to lower frequencies and, more important, the intensity of the 1350 cm^{-1} feature becomes six times larger than the one of the 1354 cm^{-1}

Table 3.4. Main IR peaks (in cm^{-1}) for CH_3CCD and CD_3CCH on Cu(111):4x√3 unit cell

vibrational	CH_3CCD		vibrational	CD_3CCH	
mode	ω_i	I_i[a]	mode	ω_i	I_i[a]
CD st	2157/2161	1.3/1.6	CH st	2930/2935	3/5
CH_3 as st	3008/3017	0.1/0.2	CD_3 as st	2224/2232	0.1/0.2
CH_3 as-s st	2989/2992	0.6/1.6	CD_3 as-s st	2210/2212	1/2
CH_3 s st	2918/2921	5/29	CD_3 s st	2097/2098	2/12
C^1–C^2 st – CH_3 s df	1342/1347	6/2	C^1–C^2 st	1345/1351	2/1.6
CH_3 as df	1413/1422	0/0	CD_3 as df	1014/1017	1/0.1
CH_3 as-s df	1429/1477	0/0.2	CD_3 as-s df[b]	1021/1060	0/0.3
CH_3 s df + C^1-C^2 st	1323/1328	0.4/0	CD_3 s df[b]	1046/1052	3/0

Key: as, asymmetric; s, symmetric; st, stretching; df, deformation; ro, rocking; b, bending.
[a]Intensities in $Kmmol^{-1}$. [b]the mode is coupled with the CH bi.

band. This intensity change arises from an inter-molecular coupling (see **Table 3.3**). The positive coupling ((C^1–C^2 st – CH_3 s df) + (C^1–C^2 st – CH_3 s df)) increases the dipole moment change and, consequently, the intensity. Camplin *et al.* [22] have proposed that the unit cell dimensions for Cu(111) are such that the distance between two adjacent hollow sites matches that of the C≡C bond of the chemisorbed propyne. This correspondence allows the C^1–C^2 stretch to become active at expense of the methyl deformation. Our calculations confirm and complete the experimental assignment. The MSSR-inactive C^1–C^2 st becomes active because is coupled with the CH_3 s df (i.e. the normal mode is the sum of the two functional group modes).

Upon deuteration of the 'acetylenic' hydrogen (see **Table 3.4**), there are no significant changes in the CH st mode and the frequency shift is in good agreement with the one predicted from a simple harmonic oscillator model [34]. Moreover, our calculations predict a shift down of the peak at 1350/1357 cm^{-1} of ~8 cm^{-1} in good agreement with the experimental isotopic shift [8]. This result allows us to emphasize the shortcomings of band assignation based exclusively on isotopic shifts.

Upon methyl deuteration, the CH_3 symmetric stretching frequencies shift down but the normal modes do not change (i.e. new couplings do not appear). The picture for the CH_3 deformation modes is rather more complicated. The CH_3 asymmetric deformation modes shift down to ~1000 cm^{-1} and mix with the CH bi mode (see footnotes **Table 3.4**). Besides, the 1325–1357 cm^{-1} peaks change significantly. The methyl deuteration breaks the coupling between the C^1–C^2 st and CH_3 s df modes. Two well separated bands appear with close intensities. Although the C^1–C^2 bond is almost parallel to the metal surface, the C^1–C^2 st mode is still observed (1345/1351 cm^{-1}, **Figure 3.11**). The RAIR[8] and EEL[20] spectra of acetylene adsorbed on Cu(111) also exhibit a strong band at 1294 and 1307 cm^{-1}, respectively. These features have also been assigned to the MSSR-inactive C≡C stretch.

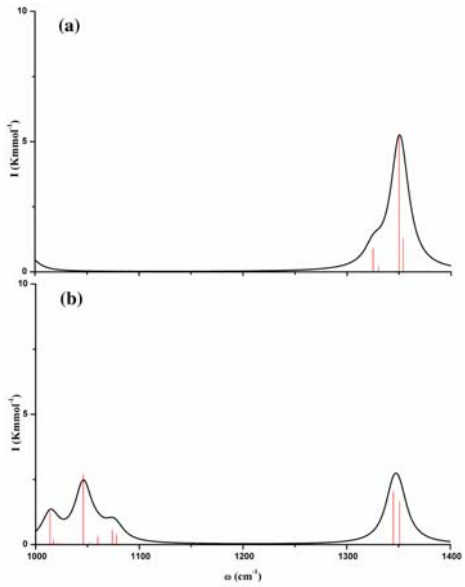

Figure 3.11. Isotopic effects on the simulated vibrational spectrum of propyne/Cu(111): 4x√3 unit cell. CH_3CCH (a), CD_3CCH (b).

Propyne on Pt(111). To our knowledge, the experimental spectrum of propyne on Pt(111) is not available. We present the calculated frequencies, RAIRS intensities and band assignment in **Table 3.5**. In the CH stretching region, the most intense feature is the CH_3 s st but CH_3 as and CH st have also a non negligible intensity. Interestingly enough, the band order is the same than that for the gas phase propyne (see **section 3.2**). The frequencies of the CH_3 stretching modes do not change significantly on adsorption but there is a great shift down of the CH st frequency. The changes in frequency are well in line with the changes in geometry.

In the 1300–1500 cm^{-1}, three features have a noteworthy intensity. We assign these peaks to the CH_3 as-s df + C^1–C^2 st (1433 cm^{-1}), CH_3 as df (1407 cm^{-1}) and CH_3 s df (1330 cm^{-1}). The feature at 1433 cm^{-1} has its counterpart at 1355 cm^{-1} (C^1–C^2 st – CH_3 as-s df), which has an intensity equal to zero.

Upon deuteration of the 'acetylenic' hydrogen, there are no significant changes in the normal modes (see **Appendix A.1**). Obviously, the CH st frequency is shifted to lower frequencies (2246 cm^{-1}). Moreover, the 1355 cm^{-1} band is shifted to 1346 cm^{-1}. This difference indicates that the 'acetylenic' hydrogen contributes to the mode. On methyl deuteration, both the CH_3 st and the CH_3 df modes are obviously shifted to lower frequencies. Only the CH_3 deformation modes change in some extent. These modes shift down to the ~1000 cm^{-1} region and mix with the C^2–C^3 st and CH bi modes (see **Appendix A.1**). Moreover, this frequency shift also breaks the coupling of the CH_3 as df modes with the C^1–C^2 st. The C^1–C^2 st mode appears at 1361 cm^{-1} but its intensity is almost negligible.

Table 3.5. Computed frequencies (in cm^{-1}) for propyne (CH_3CCH) on Pt(111) and Pd(111): 2x2 unit cell

vibrational	Pt(111)		vibrational	Pd(111)	
mode	ω_i	I_i^a	mode	ω_i	I_i^a
CH st	3049	1.4	CH st	3045	0.9
CH_3 as st	3028	0.6	CH_3 as st	3016	0.6
CH_3 as-s st	3011	2.0	CH_3 as-s st	3004	2.5
CH_3 s st	2934	7.2	CH_3 s st	2935	9.1
CH_3 as-s df + C^1–C^2 st	1433	0.7	CH_3 as-s df + C^1–C^2 st	1439	0.7
CH_3 as df	1407	2.0	CH_3 as df	1405	0.5
C^1–C^2 st – CH_3 as-s df	1335	0.0	C^1–C^2 st – CH_3 as-s df	1394	0.9
CH_3 s df	1330	1.6	CH_3 s df	1327	0.8

Key: as, asymmetric; s, symmetric; st, stretching; df, deformation; ro, rocking; b, bending.
[a]IR intensities in $kmmol^{-1}$.

Propyne on Pd(111). The computed spectrum for propyne on Pd(111) is similar to that on Pt(111) (see **Table 3.5**). In the CH stretching region, there are no major differences between the two metal surfaces in both frequencies and intensities. However, there are some significant changes in the 1300–1500 cm^{-1} region. The CH_3 as-s df and CH_3 as df modes appear at 1439 and 1405 cm^{-1}, respectively. These two modes mix in some extent with the C^1–C^2 st (see **Table 3.5**). Moreover, we assign the 1394 cm^{-1} feature to the C^1–C^2 st + CH_3 as-s df mode. This peak has an intensity different from zero due to the positive sign of the coupling. The peak at 1327 cm^{-1} corresponds to the CH_3 s df mode.

Upon deuteration, the changes are analogous to those observed on Pt(111) (see **Appendix A.2**).

Propyne on Rh(111). The experimental HREELS spectrum of propyne on Rh(111) [14] shows five broad peaks at: 2930, 1445, 1370, 1115 and 1005 cm^{-1}. The 2930 cm^{-1} feature is the most intense band in the spectrum. The peaks at 1445, 1370 and 1005 cm^{-1} have rather similar intensities (~2/3 of the intensity of the main peak) and the 1115 cm^{-1} feature is the less intense signal (~1/2 of the intensity of the 2930 cm^{-1} band). Somorjai and co-workers [14] have interpreted this spectrum by comparison with the gas-phase IR spectrum of propyne. They have assigned the bands at 2930, 1445, 1370, 1115 and 1005 cm^{-1} to the CH_3 as st, CH_3 as df, CH_3 s df, C^1C^2 st and CH_3 ro, respectively.

Table 3.6 shows the calculated vibrational frequencies, HREELS intensities and band assignment for the two surface minima on Rh (see **section 3.3.1**): hcp-par and bri-perp'. **Figure 3.12a-b** illustrates the simulated HREEL spectra. The overall agreement between experimental and theoretical spectrum is better in the case of the hcp-par structure. The peaks at 2930, 1445 and 1370 cm^{-1} appear among the frequencies of the two minima. We assign the feature at 2936/2936 cm^{-1} to the CH_3 s st, the one at 1432/1409 cm^{-1} to the CH_3 as df and the peak at 1330/1324 cm^{-1} to the CH_3 s df . Here, the values correspond to the hcp-par/bri-per' minima, respectively (see **Table 3.6**). We disagree with the assignment of

Table 3.6. Computed frequencies (in cm^{-1}) for propyne (CH_3CCH) on Rh(111): 2x2 unit cell

vibrational mode	hcp-par ω_i	hcp-par I_i[a]	vibrational mode	bri-per ω_i	bri-per I_i[a]
CH st	3035	0.2	CH_3 as st	3035	0.1
CH_3 as st	3018	0.2	CH_3 as-s st	3001	0.0
CH_3 as-s st	3005	0.6	CH st	2963	0.4
CH_3 s st	2936	2.9	CH_3 s st	2936	2.0
CH_3 as-s df + C_1–C_2 st	1432	0.1	CH_3 as-s df	1431	0.1
CH_3 as df	1411	1.1	CH_3 as-s df	1409	0.9
CH_3 s df	1330	1.1	CH_3 as df	1324	1.6
C^1–C^2 st – CH_3 as-s df	1323	0.0	C^1-C^2 st	1207	0.1
CH_3 s ro + CH bi	1083	0.2	CH_3 s ro – CH bi	1063	1.1
CH bi – CH_3 s ro	988	1.4	CH_3 as ro	958	0.3
CH_3 s ro	978	0.2	CH bi + CH_3 s ro	952	0.0
C^2– C^3 st	907	0.7	C^2– C^3 st	841	1.1
CH bo	749	0.8	CH bo	779	0.0

Key: as, asymmetric; s, symmetric; st, stretching; df, deformation; ro, rocking; b, bending.
[a]HREELS intensities computed following the experimental setting in ref 14.

the ~2930 cm^{-1} band in ref [14]. However, the band intensities of the hcp-par spectra are closer to the experimental values than the ones of the bri-perp spectrum. In the latter, the peak at 1324 cm^{-1} is obviously more intense than the feature at 1409 cm^{-1} whereas on the experimental spectrum these two peaks have similar intensities. The bands at 1115 cm^{-1} and 1005 cm^{-1} are also in better agreement with the frequencies of the hcp-par structure. However, we disagree with the experimental band assignment. For the hcp-par adsorption mode, we assign the features at 1083 and 988 cm^{-1} to the negative and positive coupling between the CH_3 s ro and the CH bi. The picture is similar for the bri-perp structure. We assign the bands at 1063 cm^{-1} and 958 cm^{-1} to the (CH3 s ro + CH bi) and to the CH_3 as ro, respectively. Actually, the differences between the experimental and the theoretical values are smaller than 32 cm^{-1} for the hcp-par mode whereas they are of 52 cm^{-1} and 47 cm^{-1} for the bri-perp structure (see **Table 3.6**). However, the theoretical intensities do not match well with the experiment. Our calculations predict two bands with very different intensities in this region for both minima while the differences in the experimental spectrum are not so important (see below).

Besides, the spectrum of the bri-perp' surface structure has a quite strong peak at 841 cm^{-1} not present in the experimental one. The differences between the experimental and the computed bri-perp' spectra are big enough to rule out this adsorption mode as the majority species on the surface but they are not sufficient to exclude its presence on the surface.

To study how the presence of these two adsorption modes on the surface can change the appearance of the spectrum, we calculated the hcp-per and bri-perp' modes co-adsorbed on a 2x4 unit cell. Unfortunately, during the geometry optimisation the bri-perp structure

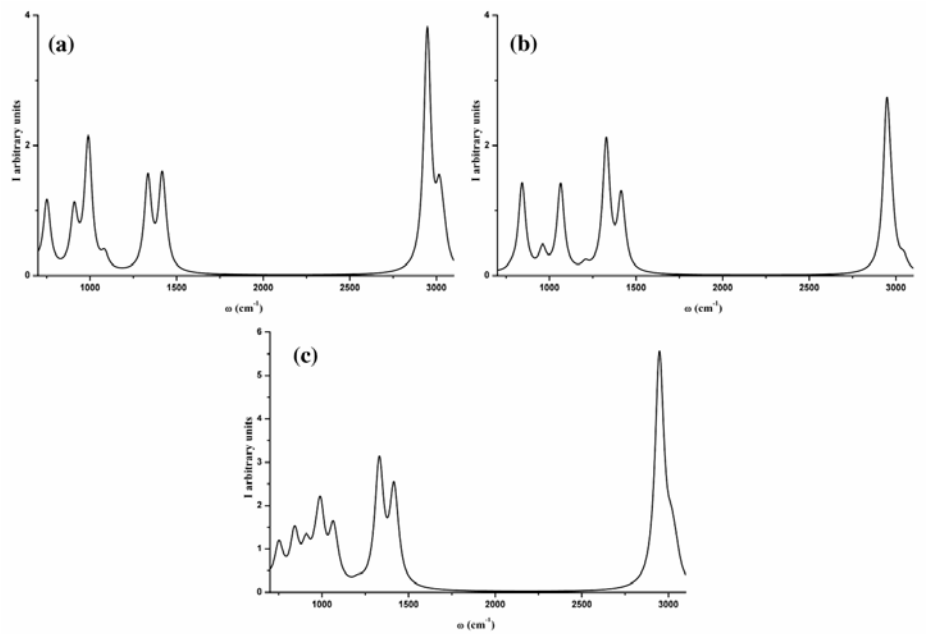

Figure 3.12. Simulated HREELS spectra for propyne adsorbed on Rh(111): hcp-par mode (a), bri-perp' mode (b) and sum of the spectra of the two posible surface structures.

evolved to the hcp-par mode, which indicates that this surface overlayer is not stable. The use of a large unit cell (e.g a 4x4 supercell with four adsorbed molecules) is prohibitively expensive. This is one of the shortcomings of the slab model. Thus, we simulated the vibrational spectrum as a sum of the spectrum obtained for each mode separately (see **Figure 3.12-c**). Notice that the coupling between adsorbed molecules is neglected. Moreover, the ratio hcp-par/bri-perp' is 1/1. Despite the limitations of this approximation, we observe a quite interesting conclusion. The presence of the bri-perp' structure increases the intensity of the band at ~1100 cm^{-1}. This fact allows us to conclude that the hcp-par structure covers the Rh(111) surface but there is a small proportion of bri-perp' adsorbed molecules. The results from the simulation of the vibrational spectra support the conclusions inferred from electronic energy calculations.

We considered it interesting to focus our attention on the MSSR-inactive C^1–C^2 st mode. For sake of comparison, we analyse the changes in the RAIRS intensities. For the hcp-par structure, this mode appears at 1323 cm^{-1} coupled with the CH_3 as df. For the bri-perp adsorption mode, it appears at 1207 cm^{-1}. For both minima, the C^1–C^2 st has an intensity close to zero (< 0.1 $kmmol^{-1}$). Upon methyl deuteration, the normal mode changes but frequencies do not (differences < 5 cm^{-1}). Only the intensity of the bri-perp' C^1–C^2 st increases slightly (up to ~ 0.3 $kmmol^{-1}$).

In the first place, we compare the spectra of the hollow parallel structures (Pt, Pd and Rh). We do not observe important differences in the CH stretching region. On the 1300–1500 cm^{-1} range, we focus our attention on the C^1–C^2 st mode. We observe that the C^1–C^2 stretch couples with the CH_3 asymmetric deformation in all the cases. Upon methyl deuteration, this coupling disappears but the changes in both intensities and frequencies are not very important. The C^1–C^2 st mode appears at 1361 cm^{-1} for Pt, 1410 cm^{-1} for Pd and 1325 cm^{-1} for Rh. These values are in good agreement with the molecular distortion predicted by our calculations (see **Figure 3.5**). Unfortunately, the intensity of this feature is almost zero and it cannot be used to identify the adsorption structure from experiments.

For the bri-perp minima (Cu and Rh), there are no outstanding differences in the 2900–3100 cm^{-1} region. On the other hand, the C^1–C^2 st couples strongly with the CH_3 s df on Cu whereas this mode is almost pure on Rh. On methyl deuteration, the coupling observed on Cu disappears. The C^1–C^2 st appear at 1357 cm^{-1} on Cu and 1203 cm^{-1} on Rh. Again, calculated frequencies are well in line with predicted geometries.

Finally, we compare the hollow-par spectra with the bri-perp results. There are considerable differences. In the spectra of the hollow-par minima the CH st appears at higher frequencies than in that of bri-perp structures. This is not surprising because propyne is more activated in the bri-perp adsorption modes (i.e. the distortion energy of the molecules is higher than in the hollow parallel minima).

However, the intensity of the C^1–C^2 st mode illustrates the most remarkable difference. Notice that we compare the spectra for CD_3CCH. For hollow parallel modes this feature is not active (intensity < 0.1 $kmmol^{-1}$). On the other hand, for bri-per structures this mode is active. The intensity of the C^1–C^2 st is very low for propyne on Rh but it is quite important on Cu. In the former, the molecule interacts predominantly with the d-band while in the latter the sp-band plays the main role. The delocalised nature of the sp electrons may increase the electronic density around the C^1–C^2 and cause this mode to be infrared active. McCash and co-workers [4,8] proposed that for acetylene on Cu(111) the changes in the electron density in the C≡C bond due to its stretching mode are enough to make this mode MSSR-active.

3.4 Conclusions

We studied the adsorption of propyne on the (111) surface of Cu, Pt, Pd and Rh by means of DFT periodic calculations. We investigated several possible adsorption modes and determined that the most stable adsorption geometry is the bridge-perpendicular configuration (di-σ/di-π) for Cu(111) and the hollow-parallel adsorption mode (di-σ/π) for Pt(111), Pd(111) and Rh(111). Besides, on the Rh(111) surface we found that the bri-perp structure is close in energy to the most stable one. Our results are in agreement with the experimental data available.

We explained the variation of the adsorption energies on Cu (–98 $kJmol^{-1}$), Pt(–197 $kJmol^{-1}$), Pd(–161 $kJmol^{-1}$) and Rh (–226 $kJmol^{-1}$) and the exceptional behaviour of Cu(111) in terms of geometric distortions and electronic interaction.

The decomposition of the adsorption energy in its main contributions was not conclusive but shed light on the reasons for the different reactivity of propyne on these surfaces. The strong interaction of propyne with Pt and Rh favours probably its decomposition. However, on Pd(111) and Cu(111) further analysis of the reaction intermediates and possible reaction pathways is necessary to understand the differences observed.

The analysis of the projected density of states (PDOS) allowed us to conclude that the interaction between the π system of propyne and the d-band of the metal is better on Rh, than on Pt, than on Pd, than on Cu, because of the filling and shape of the d-band. We also observed that propyne mainly interacts with the sp-band of Cu. These findings helped us to understand the trends in adsorption energies and the unique behaviour of Cu. We attributed the singular adsorption behaviour of propyne on Cu to the high degree of overlap of Cu 4s band with the π antibonding orbitals of propyne.

For propyne on Cu and Rh, calculated vibrational spectra permitted us to reproduce the experimental spectra with a very good fit. Computed frequencies confirm the results obtained from electronic energy calculations. We corroborate the presence of the MSSR-inactive C≡C stretching mode in the spectrum of propyne on Cu and give and explanation for this result. The C≡C st mixes with the CH_3 s df. This coupling causes an increase of the dynamic dipole moment perpendicular to the surface. On methyl deuteration, this coupling disappears but the changes in the electron density near the C≡C are enough to create a significant dipole moment perpendicular to surface. Consequently, the mode is IR active. Moreover, on Rh the analysis of the simulated spectrum and the comparison with the HREELS data led to a co-adsorption of propyne in both surface structures (hcp-par and bri-perp'), with larger proportion of the hollow parallel adsorption mode. Calculations also allowed us to predict the vibrational bands for propyne on Pt(111) and Pd(111).

3.5 References and Notes

[1] J. Ryczkowski, *Cat. Today* 68 (2001) 263.
[2] N. Sheppard, *Ann. Rev. Phys. Chem.* 39 (1988) 589.
[3] P. Hollins, J. Pritchard, *Prog. in Surf. Sci.* 19 (1985) 275.
[4] E.M. McCash, Surface Chemistry, Oxford University Press Inc., New York (2001).
[5] D.P, Woodruff, T.A. Delchar, *Modern Techniques of Surface Science*, 2ond Ed., Cambridge Solid State Science Series, Cambridge University Press, Cambridge (1994).
[6] N. Shepard, C. De La Cruz, *Cat. Today* 70 (2001) 3.
[7] I.N. Levine, *Molecular Spectroscopy*, John Wiley &Sons, Inc., New York (1975) 268.
[8] M.A. Chesters, E.M. McCash, *J. Elec. Spec. Relat. Phenom.* 44 (1987) 99.
[9] A. Markovits, M. García-Hernández, J.M. Ricart, F. Illas, *J. Phys. Chem. B* 103 (1999) 509.
[10] R.G. Greenler, *J. Chem. Phys.* 44 (1966) 310.
[11] H.A. Pearce, N. Sheppard, *Surf. Sci.* 59 (1976) 205.
[12] T. M. Gentle, E.L. Muetterties, *J. Phys. Chem.* 87 (1983) 2469.
[13] J.W. Peck, D.I. Mahon, B.E. Koel, *Surf. Sci.* 410 (1998) 200.
[14] B.E. Bent, C.M. Mate, J.E. Crowell, B.E. Koel, G.A. Somorjai, *J. Phys. Chem.* 91(1987)1493.
[15] R.L. Middleton, R.M. Lambert, *Catal. Lett.* 59 (1999) 15.

[16] R.L. Toomes, R. Lindsay, P. Baumgärtel, R. Terborg, J.-T. Hoeft, A. Koebbel, O. Schaff, M. Polcik, J. Robinson, D.P. Woodruff, A.M. Bradshaw, R.M. Lambert, *J. Chem. Phys.* 112 (2000) 7591.
[17] A. Clotet, J.M. Ricart, F. Illas, G. Pacchioni, R.M. Lambert, *J. Am. Chem. Soc.* 122 (2000) 7573.
[18] C.J. Ennis, P.A. Carr, E.M. McCash, *Surf. Sci.* 539 (2003) L574.
[19] R.J. Koestner, J.C. Frost, P.C. Stair, M.A. van Hove, G.A. Somorjai, *Surf. Sci.* 116 (1982) 85.
[20] B.J. Bandy, M.A. Chesters, M.E. Pemble, G.S. MacDougall N. Shepard, *Surf. Sci.* 139 (1984) 87.
[21] A.J. Roberts, S. Haq, R. Raval, *J. Chem. Soc. Faraday Trans.* 92 (1996) 4823.
[22] J.P. Camplin, J.K. Eve, E.M. McCash, *Phys. Chem. Chem. Phys.* 2 (2000) 4433.
[23] M.I. El Idrissi, J. Liévin, M. Herman, A. Campargue, G. Graner, Chem. Phys. 265 (2001) 273.
[24] T.Shimanouchi, *Tables on Molecular Vibrational Frequencies*, National Standard Reference Data Series, National Bureau of Standards, Washington, DC (1972) and references therein.
[25] A.Clotet, G. Pacchioni, *Surf. Sci.* 346 (1996) 91.
[26] We used a 4x√3 unit cell and a 2x√3 model.
[27] J. W. Medlin, M.D. Allendorf, *J. Phys. Chem. B* 107 (2003) 217.
[28] F. Delbecq, P. Sautet, *J. Catal.* 211 (2002) 398.
[29] F. Mittendorfer, C. Thomazeau, P. Raybaud, H. Thoulhoat, *J. Phys. Chem. B* 107 (2003) 12287.
[30] C. J. Baddeley, A. F. Lee, R. M. Lambert, T. Giessel, O. Schaff, V. Fernandez, K. -M. Schindler, A. Theobald, C. J. Hirschmugl, R. Lindsay, A. M. Bradshaw, D. P. Woodruff, *Surf. Sci.* 400 (1998) 166.
[31] M. Mavrikakis, J. Rempel, J. Greeley, L.B. Hansen, J.K. Norskov, *J. Chem. Phys.* 117 (2002) 6737.
[32] A. Gil, A. Clotet, J.M. Ricart, G. Kresse, M. García-Hernandez, N. Rösch, P. Sautet, *Surf. Sci.* 530 (2003) 71.
[33] R. Hoffmann, *Angew. Chem. Int. Ed. Engl.* 26 (1987) 846.
[34] Isotopic factor, ωD/ωH= 1.35–1.39.